Bulg. J. Phys. **45** (2018) 299–312

Investigation of Inelastic Cross Sections for pp and $p\bar{p}$ Collisions Using RBF Intelligent Computing Approach

El-Sayed A. El-Dahshan[1,2]
[1]Department of Physics, Faculty of Sciences, Ain Shams University, Abbassia, 11566, Cairo, Egypt
[2]Egyptian E-Learning University (EELU), 33 Elmesah Street, Eldoki, 11261, El-Geiza, Egypt

Received: *March 12, 2018*

Abstract. The inelastic cross-section is an important observable in high and ultra-high-energy cosmic rays and hadronic interactions. In the present work, radial basis functions (RBF)-based intelligent computing (IC) model is presented for modeling the inelastic cross-sections of both pp and $p\bar{p}$ collisions (σ_{inels}) from low to ultra-high energy (from below the ISR to the most recent LHC). Radial basis functions (RBF) neural networks are intelligent and powerful algorithms that can be used for function approximation and nonlinear modeling. The RBF-based IC model has been developed and trained, based on the available experiment to model (and approximate) the inelastic cross-section data of both pp and $p\bar{p}$ collisions as a function of center-of-mass-energy ($\sqrt{s}$). Our obtained results of σ_{inels} for pp and $p\bar{p}$ are compared with other theoretical calculations and predictions. It is found that the calculated and predicted cross-sections highly agree with both the available experimental measurements and theoretical results as well as the predictions of the other models. The results of our developed model show a good performance in modeling the experimental data and prediction for the unseen values of σ_{inels}.

PACS codes: 95.30.Cq, 13.60.Hb, 95.75.Pq, 07.05.Mh, 07.05.Tp

1 Introduction

The hadronic cross-sections are fundamental observables in particle physics. They have been studied in many experiments, as well as empirical and semi-empirical models (phenomenological models), covering several orders of magnitude in centre-of-mass energy ($\sqrt{s}$). In addition to their real subdivisions into elastic σ_{el} and inelastic σ_{inels} contributions, total hadronic (proton-proton) cross-sections σ_{tot} involve principal quantities that have been considered in high-energy particle (HEP) experiments and cosmic-ray (CR) physics over the former

(nearly) seventy years [1-5]. The σ_{inel} is an essential observable for proton interactions, however, it cannot be figured and calculated from first principles; since quantum chromodynamics cannot yet be understood for delicate procedures. In 1973, the experimental results at CERN discovered that σ_{tot} rises with energy "$\sqrt{s}$" as Heisenberg had predicted [6-8].

Phenomenological and empirical models of particle physics suppose a logarithmic growing of the inelastic cross-section with energy "$\sqrt{s}$" uses a power law dependence [1,9] while not exceeding the Froissart-Martin bound [8,10], which is asymptotically behavior and power law depending on $\ln(s)$ [9,11].

Theoretical models for the non-perturbative methods and diffractive scattering have been developed and executed into Monte Carlo (MC) simulation and event generators [12-14] to describe the interactions and the hadronization process of the partonic interactions final state. The measurement and investigation of the inelastic proton-proton (pp) and proton-ant-proton ($p\bar{p}$) cross-section at the most probable collision energy used as input to these models, and is essential for investigating the validity and tuning of such models [12].

The early measurements were performed at fixed target experiments at the very low (at BNL [1950s] and at Serpukhov [1967]), CERN energies, Synchro-Cyclotron (SC) [1957] and Proton Synchotron (PS) [1960] colliders. They were followed by colliding beams measurements at the Intersecting Storage Ring (ISR) [1971] and Super Proton Synchotron (SPS) [1974]. Several Tevatron experiments [1985] measured the cross-section at a center-of-mass energy of 1.8 TeV. Then, they were followed by [15-17] and other antiproton accelerators – Large Electron Positron Collider (LEP) (1987) – Large Hadron Collider (LHC) (2008).

Increase of the pp total cross-section and their subdivisions (elastic and inelastic) with energy has been discovered since the first results of the Intersecting Storage Ring (ISR) at CERN in the 70s [7]. The CERN $s\bar{p}ps$ Collider (1985) found this rising valid for the pp total cross-section as well [1,4,9], and this was confirmed at FermiLab accelerator. The highest energies were and are still available only in cosmic rays: Cosmic ray (CR) measurements indicated in 1972 that the pp total cross-section was rising as the energy increased) [1,18-21].

However, the actual energy dependence of the inelastic hadronic cross-section is still an open question of intense theoretical interest. Variety of models, theoretical and empirical, has been established to study the subject [13-14].

Depending on the benefits of the artificial neural networks (ANN) [22], which include an capability to implicitly find complicated non-linear correlations amongst dependent and independent variables, ANN have been used to model and simulate many physical phenomena in particle physics [23-32].

Since the last decade, researchers have been using artificial intelligence (AI) and ANN for predicting, investigating and controlling the HEP results and experi-

ments [27-32]. The ANN models require only a dataset consisting of process parameters and corresponding HEP experiment values. RBF is one of the most powerful types of ANN [33-35]. The ANN models require only a dataset consisting of process parameters and corresponding HEP experiment values. RBF is one of the most powerful types of ANN [36-37]. Mathematically, RBF is function approximator, where the unknown function is approximated by a linear combination of a set of basis (kernel) functions (radial basis functions), given a set of data points. The application of RBF for function approximation (Intelligent computing modeling) is motivated by the lack of knowledge about the underlying physical phenomena.

Many physics results will be presented as a direct product from the successful application of different RBF algorithms in non-linear phenomena in physics and sciences. For example, G. Carleo and M. Troyer [38] have affirmed that ANN–based methodologies can be effectively utilized to solve the quantum many-body issue, for ground-state properties as well as for modeling the evolution produced by a complicated set of excited quantum states. P. Teng [39] has used the RBF network to demonstrate the wave-function as the variational wave-function for the ground state of a quantum system. J.S. Zheng [40] has applied the RBF approach to study and predict the nuclear mass. V.I. Gorbachenko [41] has proposed RBF model to deal with the boundary value problems of mathematical physics. F. Bonanno [42] has examined the use of an advanced ANN-based model of a module to achieve a highly precision of the predicted output current–voltage and power–voltage curves and to keep in account the change of every one of the parameters at various working conditions. S. Elanayar [43] has introduced a way to approximate the dynamic and static equations of stochastic nonlinear systems and to infer state variables in view of RBF-based neural network (RBFNN). Others interested applications of the RBF approach to investigate many physics phenomena have been found in [44-49]. The success of the RBF methods in the above mentioned fields encourages us to use it in modeling and investigating the behavior of pp scattering.

In the present study, the RBF function approximator (intelligent computing "IC" model) is employed to simulate and model the experimental data of σ_{inels} for pp and $p\bar{p}$ [1-3,6,8,11,15-20]. Specifically, in this paper, RBF model developed herein is mainly aimed at generating mathematical approximator functions for the calculation and prediction of the inelastic cross-sections of both pp and $p\bar{p}$ scattering (σ_{inels}) from very low to extremely-high energy energies (from fixed target experiments below the ISR to the recent LHC highest available energy of 8 TeV of LHC, up to 14 TeV).

The rest of the article is structured as follows: Section 2 presents details of the application of ANN technique via RBF approach to model the inelastic cross-sections of both pp and $p\bar{p}$ collisions (σ_{inels}) from very low to ultra-high energy regions and their energy dependence. The results obtained and their discussions are discussed in Section 3. Finally, Section 4 provides the findings and conclusions.

2 Intelligent Computing Model for Inelastic pp and $p\bar{p}$ Cross-Sections

The aim of this study is to develop an intelligent computing (IC) model to simulate and model the inelastic cross-sections of both pp and $p\bar{p}$ collisions (σ_{inels}) from very low to extremely-high energy regions (from below the ISR to the most recent LHC). To achieve this aim, the RBF neural networks approach can be used to find the approximation solution of the pp and $p\bar{p}$ inelastic cross-sections (σ_{inels}) for describing the given experimental data [1-3,6,8,11,15-20]. The objective of RBF modeling problem is to approximate a suitable mathematical model (approximator function) that can approximately express the behavior of non-linear complex system (in our case σ_{inels} for pp and $p\bar{p}$) directly from the experimental data [1-3,6,8,11,15-20]. DTREG software [50] is used for the RBF-based IC model, using an evolutionary method called repeating weighted boosting search (RWBS) and k-fold cross-validation [51-52] techniques for producing highly accurate results and assessing the accuracy of the model without requiring an independent test dataset. In order that locate how exact the results of the developed models are, some statistical performance metrics are used [53].

2.1 RBF neural network overview

In this paper, we will use another type of ANN which is called RBF [33-35]. These networks have the advantage of being much simpler than the perceptrons, while keeping the major property of universal approximation of functions [33-35]. RBFs rank among the most popular tools for function approximation and have currently been broadly applied in numerous physics-based models and data models, such as non-linear system control, non-linear function approximation, and optimization [36-48]. The RBF network is particular type of ANN that uses radial basis functions as mapping kernels. Although several forms of radial basis may be used, Gaussian kernels are most commonly used [33-37]. The present work focuses on the capability of the RBF to accomplish the function approximation and intelligent computing task instead of learning only the exhaustive training data presented to the network.

The generic topology of an RBF network is depicted in Figure 1. The RBF architecture consists of three layers: the 1$^{\text{st}}$ layer is an input layer, the 2$^{\text{nd}}$ layer is a hidden (kernel) layer and the final one is the output (summation) layer; as shown in Figure 1. The nodes within each layer are fully connected to the previous layer. Each of the input variables is assigned to a node in an input layer and passes directly to the hidden layer with no connection weights. The hidden nodes or units contain the Gaussian-based radial basis kernel functions (RBF), likewise called kernel functions that calculate the separations among the input vector and the center of each function. In the output layer, every node (neuron) receives the outputs of all nodes in the hidden layer, and the output of the i$^{\text{th}}$

output node is the linear composition of the final net activation. When RBF approach is applied to the problem of regression, the unknown function $f(x)$ to be fitted can be directly approximated from the training data (obtainable experimental data) based on the learning algorithm (as shown below in this section). Note that the calculation at the inside layer is non- linear, however at the final layer is linear; i.e., this is a hybrid training (learning) approach. The degree of precision of the RBF networks can be controlled by its parameters (three parameters, its "position", "spread" and "the weight" of connections). The RBF parameters for approximation can be found by the learning of the RBF centers and widths, alongside the second layer weights as versatile parameters to be determined by minimization of an error (cost) function.

During the building and training of the model, the RBF learns an approximation for the actual input-output relationship, based on the presented training dataset (experimental data).

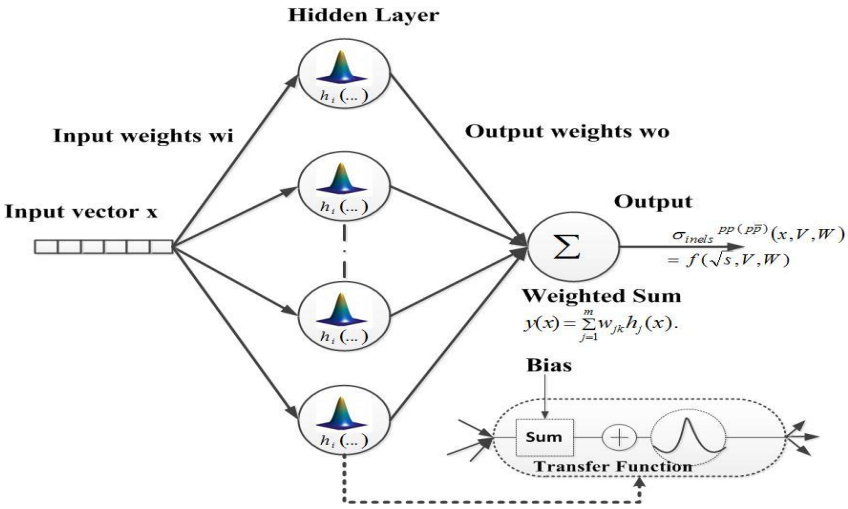

Figure 1. The RBF neural network.

Given a set of experimental data points, $\{X_i, Y_i\}_{i=1}^{i=p}$, where the vector X is an input, the vector Y is a desired output and N is the number of training pairs (experimental data) – to describe the experimental data. Based on the RBF, it is desired to construct an approximation function $\hat{Y} = f(X) \cong Y$, which reduces the error "E" (based on error function, in this case "E" is the mean square error "MSE") through the obtainable experimental data. This is in order to construct a learning method that limits "E" by adaptively updating and optimizing the three parameters of the RBF network. This approximation function $f(X)$ is assumed to be a linear weighted sum of radially symmetric function of X. Such RBF

network can be elucidate by the following model:

$$y_i(x) = \sum_{j=1}^{m} w_{ij} h_j(x : r_j, \mu_j) = \sum_{j=1}^{m} w_{ij} \exp\Big\{ -\frac{1}{2}(x_p - \mu_j)^T \Sigma_j^{-1}(x_p - \mu_j)\Big\}. \quad (1)$$

x_p is the p^{th} input vector, where w_{ij} is the synaptic weight connecting hidden neuron j to output neuron i, $h_j(\cdots)$ is a Gaussian kernel of the hidden neuron j, μ_j and $\Sigma_j^{-1}(\cdots)$ are respectively the mean vector (represents the centers μ_j) and covariance matrix (models the structure of the kernel function "spreads r_j") related to the j^{th} hidden node. Specifically, the covariance matrix is an exceptional diagonal matrix $\Sigma = r^2 I = diag(\ldots, r^2, \ldots)$, and the kernel function ends up isotropic as $h_j(x) = ||x - \mu||^2 / r_j^2$, where $||\cdot||$ denotes the Euclidean norm.

The training and parameters adjusting of RBF neural network requires the determination of the RBF parameters (the number of neurons, the central positions, width for each node "neuron" in the inside layer, and the connection weights applied to the RBF function) by reducing the quadratic error function in least square sense. The quadratic error function is of the form,

$$\varepsilon = \frac{1}{2} \sum_{k=1}^{N} \left(t \arg et - f(w, x)\right)^2 . \quad (2)$$

Learning RBF neural networks happens in two separate phases (unsupervised phase and supervised phase). The first phase is subdivided into two points: Selection of the basis function centers locations, trailed by selection of the width of each basis function. In the second stage, the connection weights between the inside and the output layers are processed.

The first stage : different strategies can be utilized to train the RBF networks. Many clustering algorithm can be utilized to determine the RBF coordinates (the central positions and width for each node in the inside layer). On the other hand, there are some guided random search methods that can be utilized to control the parameters of the RBF function; for example the genetic algorithm (GA) and adaptive simulated annealing (ASA). Most recently, repeated weighted boosting search (RWBS) [50] has been proposed as a global optimization algorithm. RWBS is very simple and easy to perform, using a minimum programming effort. Therefore, we can perform this optimization by RWBS. It additionally determines how to quit inserting neurons to the network by checking the estimated leave-one-out cross-validation (LOOCV) error and ending when the LOOCV error starts to increment because of over-fitting. *Leave-one-out cross-validation*

(LOOVCV) is K-fold cross-validation taken to its knowing farthest, with K equal to N, the number of points in the dataset [52].

The developed approach builds the RBF units one by one, by situating and forming the RBF nodes while reducing the LOOCV error "MSE". In particular, at the n^{th} phase of the building methodology, the n^{th} RBF unit is determined by reducing MSE, with regard to the node's center vector μ_n and the diagonal covariance matrix $\Sigma_n : arg \min_{mu_n, \Sigma_n} \text{MSE}(\mu_n, \Sigma_n)$.

The next stage is to update the connection weights of the RBF Network. When the number of hidden units and the parameters of the RBFs are fixed, the radial unit activation can be obtained for each input-output pair of the learning dataset. The model parameters and complexity can be adjusted by the consideration of a penalty term to the sum of squared errors (MSE) over the learning pairs $\{(x_i, y_i)\}_{i=1}^{p}$

$$\varepsilon = \frac{1}{2} \sum_{i=1}^{p} \left((t \arg et)_i - f(x_i) \right)^2 + \lambda \sum_{j}^{m} w_j^2 \,. \tag{3}$$

This kind of penalty is known as ridge regression (RR), or weight-decay, and the parameter λ, which controls the amount of penalty, is known as the regularization parameter (has to be known a priori or estimated from the data). RR adjusts the smoothness properties of the network [51-52]. The optimal regularization λ that limits generalized cross-validation (GCV) error is computed by the iterative method [52]. If the value of λ is known then the optimal weight is $\hat{W} = A^{-1} H^T y$, where $A = H^T H + \lambda I_p$ and H is the design matrix with elements $H_{ij} = h_j(x_i)$ and I_p is the $p \times p$ identity matrix.

Finally, the approximated output $\hat{Y}$ is shown in the following equation:

$$\begin{aligned} \hat{Y} &= f(X, V, W) = f(\sqrt{s}, V, W) \\ y_i(x) &= \sum_{j}^{m} w_{ij} h_j(x, \mu_j, r_j) \,, \end{aligned} \tag{4}$$

where the vector V is the RBF parameters μ_j, r_j; W is the weight matrix.

2.2 Building an RBF approximator

Based on equation (4), the output (σ_{inels}) for pp and $p\bar{p}$ of the developed RBF-based IC model is shown by the following approximate formula as a function of:

$$\begin{aligned} \sigma_{\text{inels}}^{pp\,(p\bar{p})}(x, V, W) &= f(\sqrt{s}, V, W) \\ &= \sum_{j}^{m} w_{kj} h_j(\sqrt{s}, \mu_j, r_j) \,, \end{aligned} \tag{5}$$

where $\sqrt{s}$, $V(\mu, r)$, W and σ_{inels} are as introduced above (Section 2.1).

The RBF-based IC model is completely specified by choosing its parameters vector V (the radial basis function numbers, the centers and width of each radial basis function and the connection weights w_{kj} between j^{th} hidden layer unit and k^{th} output unit). The best number of nodes in the inside layer is related to the complexity of experimental data (training data). As mentioned in the above Section 2.1, the parameters of the RBF kernel were determined by adopting the RWBS based on minimizing the LOOCV criteria. Likewise, the calculation of the best possible connection weights between the nodes in the inside layer and the final (summation) layer is performed utilizing ridge regression [52]. In the view of the regularization method, the best possible regularization lambda parameter (λ) that minimizes generalized cross-validation (GCV) error is resolved utilizing the iterative procedure developed by M. Orr [52].

The acceptance of IC mode for calculating and predicting σ_{inels} for pp and $p\bar{p}$ is based on its capability of generalizing its predictions to a new set of inputs "$\sqrt{s}$", which are not previously included in the training process.

For constructing optimal RBF-based IC models for calculating and predicting the inelastic cross-sections (σ_{inels}) for pp and $p\bar{p}$ from low to high energy regions (from below the ISR to the most recent LHC), the numbers of neurons in the inside (hidden) layer were optimized as 20 and 12, respectively. The optimal values of the radius (spread) of the respective kernel RBF for pp and $p\bar{p}$ models were 6.87, and 5.52. Minimum and maximum values of the lambda for the two models were 0.05, 0.04 (for pp) and 9.87, 9.88 (for $p\bar{p}$), respectively. The optimal values of the regularization λ for the two models were adjusted as 1.04×10^{-3} and 2.4×10^{-5}, respectively.

In order to evaluate the performances of the RBF approximator, we have taken into our consideration the statistical metrics [53]: Average Pearson correlation coefficients (CC), average NMSE (normalized mean square error (NMSE) and average mean absolute error (MAE) (between the experimental and calculated (predicted) values σ_{inels}), obtained based on the k-fold cross-validation for both training and testing data for both the RBF model. The statistical MAE, NMSE and CC values obtained for RBF-based IC model reflect that the RBF neural networks can approximate σ_{inels} for pp and $p\bar{p}$ with good accuracy and reliability.

3 Results and Discussion

In the present work, we have developed an IC model (approximated function) based on the RBF neural networks algorithm to investigate the inelastic scattering cross-section of pp and $p\bar{p}$ ($\sigma_{\text{inels}}^{pp\,(p\bar{p})}$). We have used the available experimental data [1-3,6,8,11,15-20] of the pp and $p\bar{p}$ to build and train the intelligent model. Our RBF-based IC model "RBF approximator function" (Eq. 5, $\sigma_{\text{inels}}^{pp\,(p\bar{p})}(x, V, W) = f(\sqrt{s}, , V, W)$) has been used to simulate and model the

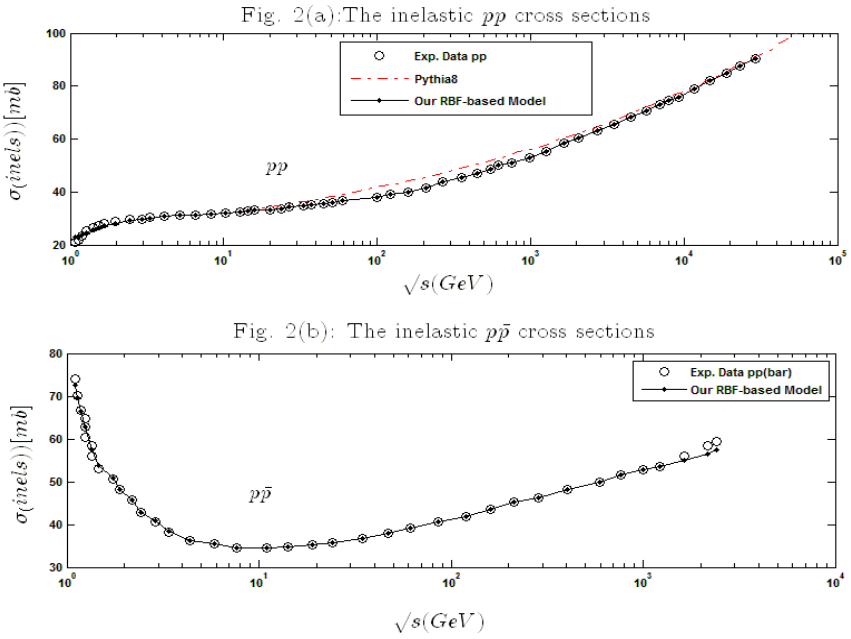

Figure 2. Comparison between our RBF-based IC model computed and predicted values (–●–) and the corresponding experimental (○) and theoretical (– –) ones for σ_{inels} of: (a) pp; and (b) $p\bar{p}$.

$\sigma_{\text{inels}}^{pp\,(p\bar{p})}$ from below the ISR to the highest LHC center of mass energy $\sqrt{s}$. The developed IC model was tested by data sets, which have not been employed in the training stage, based on the k-fold cross-validation without need for extra-data.

Figure 2 (a and b) presents the comparison between the inelastic cross-sections (σ_{inels}) of both pp and $p\bar{p}$ collisions calculated by employing our RBF-based developed intelligent model and the corresponding experimental data at the given energies. In order to evaluate the performances of the RBF-based IC model, the NMSE, MAE and CC values for both training and validation phases are given in Table 1. It is evident (from Table 1) that the optimal RBF models given up rel-

Table 1. Statistical performance of the proposed model

	Training			Validation		
	MAE	NMSE	CC	MAE	NMSE	CC
pp	0.159	0.00045	0.945	6.022	0.224	0.987
$p\bar{p}$	0.262	0.0033	0.998	10.166	2.725	0.947

(a)

(b)

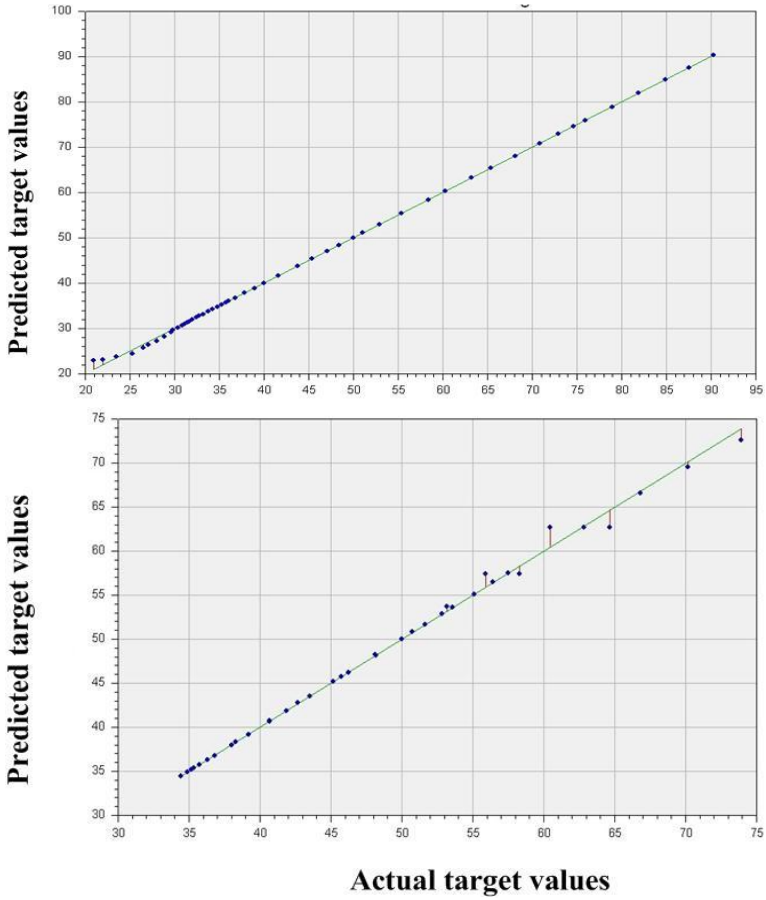

Figure 3. Pearson correlation coefficient diagram. Actual vs. predicted values: (a) pp; and (b) $p\bar{p}$.

atively higher agreement between the experimental and model estimated values of all the two dependent variables of pp and $p\bar{p}$ in the training and validation.

The performances exhibited by the proposed models used in this study may be seen in Figure 3 (Pearson correlation). It may be observed from Figure 3 (a and b) that the RBF-based model provided quite good approximation to the experimental results of the σ_{inels} for pp and $p\bar{p}$ and described the generalization performance of the RBF-based (intelligent function approximator).

The agreement between the modeled σ_{inels} for pp and $p\bar{p}$, made by RBF-based IC model and the experimental results, is especially significant. Figures 2 and 3 show that the RBF-based model is able to perfectly model and simulate the σ_{inels} of the pp and $p\bar{p}$ interactions at high energies.

In addition, it can be seen from these figures that the RBF-based model performance is satisfactory in prediction of values, compared to the experimental ones.

The RBF-based IC model has been used to compute the inelastic cross-sections at $\sqrt{s} = 7$ TeV, 8 TeV and 13 TeV, recently measured at LHC [15-56]. Comparing the RBF-based IC model computed values with the experimental data demonstrates a high generalization capability of the proposed model (see Table 2). The results prove that the proposed RBF model has impressively learned well for the complex relation between the inelastic cross-sections for pp and $p\bar{p}$ with high CC (0.945 & 0.998) and low NMSE (0.00045 & 0.0033), respectively.

Table 2. Our computation and estimation values for pp σ_{inels} (mb) compared with the corresponding experimental and theoretical ones.

		$\sigma_{inels}\,(mb)$								
		Experimental Measurements				**Our Approach – RBF-IC model**	**Other theoretical Models**			
$\sqrt{s}\,(TeV)$		**TOTEM [17, 18]**	**CMS [2, 16]**	**ATLAS [6, 8, 20]**	**ALICE [19]**		**DGM model [14]**	**Empirical model [54]**	**Pomeron and Odderon model [55]**	**M. Blok & F. Halzen [13]**
Recent LHC measurements [15-20]	**7**	**73.5 ±0.6**	**68 ± 2**	**69.4 ± 2.4**	**73.2±2.0**	**73**	**73.2**	**73.2**	**70.34 ± 2.11**	**69.0**
	8	**74.7±1.7**	**--**	**71.73±0.15**	**--**	**74**	**74.7**	**74.7**	**--**	**--**
Most recent LHC measurements [56]	**2.76**	**62.8±29**	**--**	**--**	**62.8±2.7**	**63**	**63**	**62.8**	**--**	**--**
	13	**79.5 78.8**	**71.3±0.5**	**78.1±0.9**	**--**	**78**	**80.5**	**78.1**	**---**	**--**
Near Future Measurements	**14**	**--**	**--**	**--**	**--**	**81**	**81.6**	**83.9**	**79**	**76.3**

The comparison of the experimental, theoretical and our calculated values for pp σ_{inels} is shown in Table 2. Additional, the computed and estimated values are compared to the corresponding theoretical calculations for ultra-high energies [13,14,54,55], as shown in Figure 2. From Figure 3 and Table 2, we can conclude that the prediction of σ_{inels} for pp has the same trend as the theoretical ones [13,14,54,55] which supports the ability of wide usage of our models in simulating and modeling HEP experiments. The general tendency of the computed and predicted values demonstrates a good matching with the recent LHC measurements.

4 Conclusion

RBF-based intelligent computing (IC) model is developed for modeling the inelastic cross-sections (σ_{inels}) of both pp and $p\bar{p}$ collisions from low to high energy regions (i.e. from below the ISR to most recent LHC) for the first time in this paper. We have obtained an approximator function for calculating and predicting the $\sigma_{\text{inels}}^{pp\,(p\bar{p})}$. The calculated and predicted results of our developed RBF model are compared with the results of the available experimental and theoretical models. The RBF-based IC model shows a good match to the experimental data and the other theoretical models. Moreover, our proposed model is capable of predicting experimental data for the inelastic cross-sections that are not used in the training session. Finally, it is also noticed that RBF intelligent model is very effective, which will provide a powerful approach for the precise investigation of σ_{inels}. An interesting result of this investigation is that we have a clear idea of the approximate behavior of the pp and $p\bar{p}$ as a function of the collision energy.

References

[1] D.R.O. Morrison (1973) *Proc. R. Soc. Lond. A.* **335** 461.

[2] S. Chatrchyan, *et al.* [CMS Collaboration] (2013) *Phys. Lett. B* **722** 5.

[3] K. Nakamura (2010) *J. Phys. G. Nucl. Partic.* **37** 075021.

[4] G.A. Schuler, T. Sjostrand (1994) *Phys. Rev. D* **49** 2257.

[5] G. Giacomelli (2007) "Rising total hadron-hadron cross-sections", arXiv:0712.0906 [hep-ex].

[6] A. Achilli, Y. Srivastava, R. Godbole, A. Grau, Pancheri, O. Shekhovtsova (2011) *Phys. Rev. D* **84** 094009.

[7] W. Heisenberg (1952) *Z. Phys*. **133** 65.

[8] G. Aad, *et al.* [ATLAS Collaboration] (2011) *Nat. Commun.* **2** 463.

[9] G. Pancheri, Y.N. Srivastava (2017) *Eur. Phys. J. C* **77** 150.

[10] M. Froissart (1961) *Phys. Rev.* **123** 1053.

[11] R. Aaij, *et al.* [LHCb collaboration] (2015) *J. High Energy Phys.* **2015**(2) 129.

[12] M.H. Seymour, M. Marx (2015) In: "*LHC Phenomenology*" [Springer International Publishing], pp. 287-319.

[13] M.M. Block, F. Halzen (2011) *Phys. Rev. D* **83** 077901.

[14] P.C. Beggio (2017) *J. Phys. G. Nucl. Partic.* **44** 025002.

[15] L.A. Tompkins (2011) "A Measurement of the proton-proton inelastic scattering cross-section at $\sqrt{s} = 7$ TeV with the ATLAS detector at the LHC", Ph.D Thesis, UC Berkeley.

[16] S. Valentinetti (2014) *Nuovo Cim.* **37** 193.

[17] G. Antchev, *et al.* [TOTEM Collaboration] (2013) *EPL (Europhys. Lett.)* **101** 21003.

[18] G. Antchev, *et al.* [TOTEM Collaboration] (2016) *Eur. Phys. J. C*. **76** 661.

[19] B. Abelev, *et al.* [ALICE Collaboration] (2013) *Eur. Phys. J. C.* **73** 2456.

[20] M. Aaboud, *et al.* [ALICE Collaboration] (2016) *Phys. Lett. B* **761** 158.
[21] J. Kašpar (2018) "Soft diffraction at LHC." In: *EPJ Web of Conferences*, vol. 172, p. 06005. EDP *Sciences*.
[22] S. Haykin (2008) "*Neural Networks and Learning Machines*" [Prentice Hall. New Jersey].
[23] M. Schmidt, H. Lipson (2010) In: "*Genetic Programming Theory and Practice VII*", eds. R. Riolo, U.-M. O'Reilly, and T. McConaghy [Springer US], pp. 73-85.
[24] M. Schmidt, H. Lipson (2009) *Science* **324** (5923) 81.
[25] D.J. Hills, A.M. Grütter, J.J. Hudson (2015) *Peer J. Comput. Sci.* **1**, e31.
[26] L. Todorovski, S. Dzeroski (1997) In: *Proc. 14th International Conference on Machine Learning* [Morgan Kaufmann, San Francisco, CA], pp. 376–384.
[27] C. Peterson (1990) In: *Proc. International Workshop on Software Engineering, Artificial Intelligence and Expert Systems for High Energy and Nuclear Physics*, Lyon Villeurbanne, France.
[28] A. De Angelis (1995) *Int. J. Neural Syst.* **6** 241.
[29] B. Denby (1993) *Neural Comput.* **5** 505.
[30] B. Humpert (1990) *Comput. Phys. Commun.* **56** 299.
[31] E. El-dahshan, A. Radi, M.Y. El-Bakry (2009) *Int. J. Mod. Phys. C* **20** 1817.
[32] E. El-dahshan, A. Radi, M.Y. El-Bakry (2008) *Int. J. Mod. Phys. C* **19** 1787.
[33] D.S. Broomhead, D. Lowe (1988) Radial basis functions, multi-variable functional interpolation and adaptive networks (No. RSRE-MEMO-4148). Royal Signals and Radar Establishment Malvern (United Kingdom).
[34] D.S. Broomhead, D. Lowe (1988) *Complex Systems.* **2** 321.
[35] J. Moody, C.J. Darken (1989) *Neural Comput.* **1** 281.
[36] M.D. Buhmann (2003) "*Radial Basis Functions: Theory and Implementations*" Vol. 12 [Cambridge University Press].
[37] J.A. Leonard, M.A. Kramer (1991) *IEEE Contr. Syst.* **11** 31.
[38] P. Teng, (2017) Machine learning quantum mechanics: solving quantum mechanics problems using radial basis function network, arXiv:1710.03213[quant-ph].
[39] G. Carleo, M. Troyer (2017) *Science* **355**(6325) 602.
[40] J.S. Zheng, N.Y. Wang, Z.Y. Wang, Z.M. Niu, Y.F. Niu, B. Sun (2014) *Phys. Rev. C* **90** 014303.
[41] V.I. Gorbachenko, M.V.E. Zhukov (2017) *Comp. Math. Math. Phys.* **57** 145.
[42] F. Bonanno, G. Capizzi, G. Graditi, C. Napoli, G.M. Tina (2012) *Appl. Energ.* **97** 956.
[43] Vt.S. Elanayar, C. Yung (1994) *IEEE T. Neural Networ.* **5** 594.
[44] J. Park, I.W. Sandberg (1991) *Neural Comput.* **3** 246.
[45] J.A. Leonard, M.A. Kramer, L.H. Ungar (1992) *IEEE T. Neural Networ.* **3** 624.
[46] D.K. Sonar, U.S. Dixit, D.K. Ojha (2006) *Int. J. Adv. Manuf. Technol.* **27** 661.
[47] R. Friedrich, S. Siegert, J. Peinke, S. Luck, M. Siefert, M.M. Lindemann, J. Raethjen, G. Deuschl, G. Pfister (2000) *Phys. Lett. A.* **271** 217.
[48] M.M. Li, B. Verma (2016) *Expert Syst. Appl.* **45** 161.
[49] M. Bazan, M. Aleksa S. Russenschuck (2002) *IEEE T. Magn.* **38** 1081.
[50] P. Sherrod (2008) DTREG Predictive Modeling Software, Manual for software available online: `www.dtreg.com`(Last visiting date: 08-08-2017).

[51] S. Chen, X. Wang, C.J. Harris, (2005) *IEEE T. Syst. Man. Cybern. Part B* **35** 682.

[52] J.L. Orr Mark, *Neural Comput.* (1995) **7** 606-623.

[53] G. Bohm, G. Zech (2010) *Introduction to Statistics and Measurement Analysis for Physicists* [DESY, Hamburg Germany].

[54] D.A. Fagundes, A. Grau, G. Pancheri, O. Shekhovtsova, Y.N. Srivastava (2017) *Phys. Rev. D* **96** 054010.

[55] L.L. Jenkovszky, A.I. Lengyel, D.I. Lontkovskyi (2011) *Int. J. Mod. Phys. A* **26** 4755.

[56] M. Aaboud, G. Aad, B. Abbott, J. Abdallah, O. Abdinov, B. Abeloos, R. Aben, O.S. Abou Zeid, N.L. Abraham, H. Abramowicz (2016) *Phys. Rev. let.* **117** 182002.